Dusty space plasma diagnosis using the behavior of polar mesopheric summer echoes during electron precipitation events

A. Mahmoudian[1], A. Senior[2], W. A. Scales[3], M. Kosch[4,5,6], M. T. Rietveld[7]

Abstract.

The behavior of polar mesospheric summer echoes (PMSEs) during electron precipitation event (EPE) is investigated in this paper by including dusty plasma effects for the first time. The observational data recorded with the VHF (224 MHz) and UHF (930 MHz) radars at the European Incoherent SCATter Scientific Association (EISCAT) on July 10 and 11, 2012 is presented. The observed radar echoes show that the PMSEs are both correlated and anti-correlated with the increased electron density associated with electron precipitation events in the two consecutive days. The experimental observations are compared with the numerical simulations of the temporal evolution of PMSE with different background dusty plasma parameters during EPE. Specifically, the effect of dust radius, dust density, recombination/photoionization rates, photo-detachment current, and electron density on the behavior of PMSE layer and the associated dust charging process in the course of electron precipitation events is studied. It is observed that the ratio of electron density fluctuation amplitude δn_e to the plasma density (n_e) plays a critical role in the appearance/disappearance of the layer. The simulation results revealed that the existence of PMSE is mainly determined by dust radius and dust density. The dusty plasma parameters associated with each event are estimated. The condensation nuclei of the ice particles such as proton hydrate clusters ($H^+(H_2O)_n$) or Meteoric Smoke Particles (MSP) can be determined by employing the microphysical models along with the dusty plasma simulations. This can resolve any discrepancy in the description of the observed phenomena.

1. Introduction

The natural dusty plasma formed by the disintegration of meteors appears in the atmosphere's mesosphere region between 50 and 90 km altitude. Climate change and human activity have caused decreasing mesospheric temperatures and increasing water vapor content via increased methane concentration. Noctilucent clouds (NLC) occur in the cold polar summer mesopause and are the direct visual manifestation of freezing of water vapor on the dust particles and formation of ice-coated meteoric dust particles. In-situ measurements using sounding rockets have shown deep depletion of electron density due to charging on mesospheric dust particles (e.g. Reid, 1997; Havnes et al., 2001; Rapp, 2009; Robertson et al., 2009). Accumulation of free electrons on the ice particles produces electron density structures, which cause the reflection of radar waves. Polar Mesospheric Summer Echoes PMSE are strong coherent radar echoes produced by electron density fluctuations in the vicinity of polar mesopause and at the half the radar wavelength (Rapp and Lubken, 2004). The first VHF radar echoes from the high-latitude mesosphere were observed with the Poker Flat radar in Alaska (location 65.12° N, 147.43° W) (Ecklund and Balsley, 1981; Balsley et al., 1983). The PMSE have also been observed in Antarctica (Halley station located at 76° S, 27° W) with dynasonde at 28 MHz (Jarvis et al., 2005).

Solar occultation infrared measurements have confirmed that the dust particles mainly consist of water ice in the summer polar mesosphere (Hervig et al 2001, Eremenko, et al 2005). Hervig et al (2009) reported the first measurements of mesospheric smoke particles from a satellite. The formation of the dust particles in the Earth's summer polar mesopause requires water ice nucleation and condensation as described by Rapp et al (2013). Water ice nucleation is possible from 80 to 90 km above the Earth's surface as the temperature in this altitude range drops below the water vapor frost point during the summer. The nucleation process is likely to be of a heterogeneous nature involving water ice molecules attaching to pre-existing nuclei. It has been proposed that the condensation nuclei may include large condensation proton hydrate clusters, carbon particles (i.e. soot), sulfuric acids (volcanic ash), sodium bicarbonate and hydroxide, and meteor smoke particles MSP with the latter being the most likely candidate. Extending the proton hydrate chain to large cluster sizes ($H^+(H_2O)_n$, $n > 5$) can quantify the efficiency of ionic nucleation of mesospheric ice particles. While ionic nucleation is not feasible as a major mesospheric nucleation process, it can become efficient given moderate atmospheric variations as induced by gravity waves. It should be noted that the dusty plasma formation and existence in the polar mesosphere is a very complicated that can be affected by several parameters (Christon et al., 2017).

Formation of meteoric smoke particles happens after near-complete ablation of meteoroids in the altitude range of 75-115 km and leads to particle sizes of 1–2 nm and densities of a few 1000 cm^3 as stated earlier by Hunten et al.

[1]Inter American University of Puerto Rico, Bayamon Campus, PR, USA

[2]The Bradley Department of Electrical and Computer Engineering,Virginia Tech, USA

[3]Independent Researcher, Lancaster, UK

[4]Department of Physics, University of Lancaster, Lancaster, UK

[5]South African National Space Agency, Hermanus, South Africa

[6]Dept. of Physics and Astronomy, University of the Western Cape, Bellville, South Africa.

[7]EISCAT Scientific Association, Ramfjordmoen, Norway

0148-0227/18/$9.00

(1980). The critical radius for water ice particle nucleation under typical mesospheric conditions is believed to be ≈ 1.3 nm. These particles of meteoric origin are difficult to measure and there is a relatively broad spread in the densities reported by various authors, which includes 10^1 to 10^3 cm^3 (for r_d =≈ 1nm). Gelinas et al (2005) reported the first validation of the MSPs characteristics via sounding rocket in the tropical mesosphere. The measurements show that the charged population of these meteoric particles is of the order of 100 cm^3 and the uncharged population is 1000 cm^3, which are in agreement with predictions by Hunten et al (1980). The flux of photons incident on the meteoric smoke particle surface releasing photo-electrons and ultimately resulting in positive dust particles (Havnes et al., 1990; Rapp, 2009). Therefore, photo-detachment current plays a critical role in the charging process associated with mesospheric dust in the case of proton precipitation event.

The time evolution of PMSE during perturbed atmospheric conditions such as enhanced electron density provides a unique opportunity to measure the background dusty plasma parameters. Rapp et al. (2002) presented the first investigation of PMSE dependence on background electron density during Solar Proton Event (SPE) and provided an estimation of the minimum and maximum electron density required for the PMSE observation. The negative correlation (and anti-correlation) of VHF PMSE (224 MHz) and enhanced electron density are attributed to the low dust density present within PMSE region. The increased electron density can also modify the background ion chemistry in the mesosphere. The prominent changes in the cluster ion composition, appear in N_2^+, N^+, O_2^+ and O^+. As a result, proton hydrates $H^+(H_2O)_n$, may also be produced at lower altitudes (70-85 km) and with densities ≈10^5 cm^{-3} through the fast O_2^+ chain. Another major candidate for condensation nuclei of mesospheric ice particles are large proton hydrates $H^+(H_2O)_n$. The water cluster ions increase by a factor of 100 during solar proton event, while the transition height will shift downward about 6 km in comparison with quiet ionization condition. The previous study by Rapp et al. (2002) has shown that nucleation on large proton hydrates during solar proton event is less likely due to Kelvin effect and large hydration numbers required.

Unlike the vast development of computational and theoretical models as well as experimental observations of both natural and artificially modified PMSE over the past few years (Senior et al., 2014; Scales and Mahmoudian, 2016), there are still open questions in regards to the dust charging process in the mesosphere. This paper presents the first clear variation of VHF PMSE during EPE. The slow variation of background electron density during EPE in comparison with SPE, provides an excellent condition to measure dusty plasma parameters, study formation and extinction of dust particles, and dust charging process. The main focus of this paper is the changes in the PMSE strength due to background electron density variation rather than HF heating which modifies the background electron temperature (T_e).

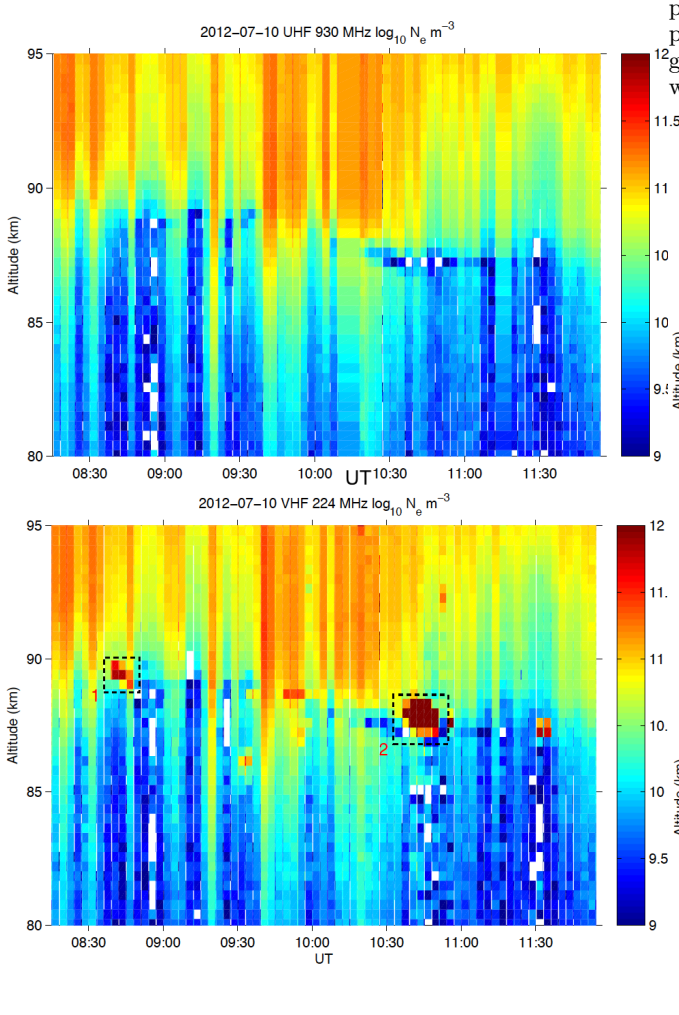

Figure 1. Experiment conducted on July 10^{th}, 2012 a) electron density measured by EISCAT UHF radar b) EISCAT VHF radar and associated PMSE layer. The black rectangles labeled 1 and 2 indicate the regions of PMSE.

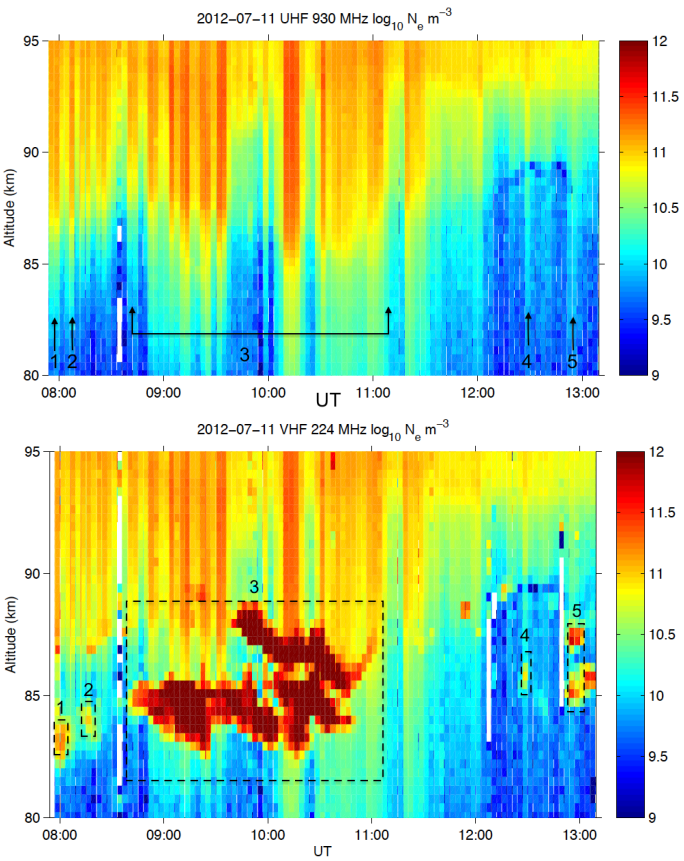

Figure 2. Repeated experiment on July 11^{th}, 2012 a) electron density measured by EISCAT UHF radar b) EISCAT VHF radar and associated PMSE layer

This paper is organized as follows. The experimental observations are presented in section 2. The computational results for the quiescent mesospheric condition and during EPE with increased electron density by factors of 10 and 20 are described in section 3. The discussion and conclusion are provided in sections 4 and 5.

2. Experimental Observations

The observations presented in this paper were recorded in two consecutive days in July 2012. The experiments started at 08:00 UT on July 10^{th} and 11^{th}, and lasted for 4 hours in each day. The electron density in PMSE region was measured by EISCAT UHF radar and the EISCAT VHF radar measured PMSE simultaneously. The electron density measured by the UHF radar between 08:00 UT to 12:00 UT, on July 10, 2012 is shown in Figure 1a. Corresponding PMSE layer measured by VHF radar is shown in Figure 1b. According to Figure 1a, two electron precipitation events are clearly seen on July 10^{th}. The first electron precipitation occurred from 08:00 to 08:45 UT and in the altitude $\sim$ 85 km. The second event is observed over a longer time period between 09:20 UT and 10:40 UT. This electron precipitation event extends to lower altitudes $\sim$ 80 km. Both cases show a maximum electron increase of the order of 10-15 during the precipitation event. The VHF radar echoes (Figure 2b) show an appearance of a weak PMSE subsequent to the precipitation event at 08:45 UT, and near the maximum electron density enhancement region $\sim$ 89 km (marked with black rectangle labeled 1). The second PMSE occurs right after the long-period precipitation event and is located in a lower altitude range of 87-88 km. This case shown with black rectangle labeled 2, stays for about 20 min and is much stronger than the case 1. The amount of energy deposited by the precipitation is quiet small even though the electron spectrum is hard. The electron temperature most likely is close to the neutral temperature (T_n). Considering the background electron density (n_e) of the order of 2×10^9 m^{-3}, the n_e enhancement ratio associated with PMSE is estimated to be about 10 based on the observations shown in Figure 1. It should be noted that some weak and scattered PMSE is observed from 09:30–10:30 UT.

Figure 2 represents the similar experimental observations carried out on July 11, 2012. In this case, a continuous electron precipitation event is detected between $\sim$08:00 UT and 12:00 UT. The precipitation event expands to lower altitudes below 85 km. The simultaneous PMSE formation extends from 83 km to 88 km and persisted for more than two hours. Unlike the earlier experiment on July 10, observations on July 11 show the coincidence of PMSE formation and electron precipitation. The electron density accumulation in PMSE region is not expected, at least not for the integration time of the radars. The VHF radar data-recording interval used in this experiment is 4.8 s. It should be noted that the HF transmitter was operating during this experiment with the heating cycle was 24 s on, 156 s off on both days. The integration time used in this study in order to resolve the heating cycles is complicated. The integration time of the radar observations presented in Figures 1 and 2, are 24 s, 153.6 s, 4.8 s, 19.2 s, 4.8 s, and 153.6 s. This arrangement is chosen to cover most of heating cycles. This is repeated for other heating cycles. This is due to the high recombination rate because of the high collision frequency. According to Figure 2a, n_e $\sim$2$\times$ 10^9 m^{-3} is considered for the background plasma in the absence of EPE. The electron density increases of the order of 10 ($\sim$ 2×10^{10} m^{-3}) in the PMSE altitude range 83–85 km from 08:00 to 08:20 UT. This period is marked with cases 1 and 2. A stronger electron precipitation event is observed from 08:50 to 11:30 UT with a maximum electron density of 5×10^{10} m^{-3} (increased by a factor of $\sim$20). This period is shown in case 3. The electron precipitation altitude extends to 80 km in case 3. Two weak events are also observed 12:30 to 12:35 UT (case 4) and 12:50 to 13:00 UT (case 5). The electron density enhancement ratio within PMSE region is estimated to be $\sim$5 in these two cases.

The appearance and weakening of PMSE shows different behavior as the background electron density changes. The cases denoted by 1–5 show the correlation of enhanced background electron density and VHF radar echoes appearance. This is mainly due to the increased background electron density above the threshold level (as well as electron density fluctuation amplitude) to scatter radar signal. The total electron density enhancement along with the radar echo intensity can be used to estimate the charging rate, and size and density of dust particles.

Figure 3 shows the proton flux measured by the GOES (Geostationary Operational Environmental Satellite) 13 satellite that shows a quiet geomagnetic condition during experiments on July 10 and 11, 2012. The technical definition of an SPE is when the 10 MeV flux exceeds 10 cm^{-2} s^{-1} sr^{-1}, the dashed horizontal line in the plot, which it fell below on 2012-07-09. Although there may have been some residual enhancement of the electron density due to solar protons on 2012-07-10, it would be weak. The radar data also show no such activities. Another characteristic of solar proton precipitation is that it tends to vary very slowly in time. Therefore, the strong and rapidly-changing enhancements in electron density shown in the radar data in Figures 1 and 2, are entirely due to energetic electron precipitation. This is of internal magnetospheric origin-electrons which have drifted around from substorm injections in the night-side and is very common at this time of day.

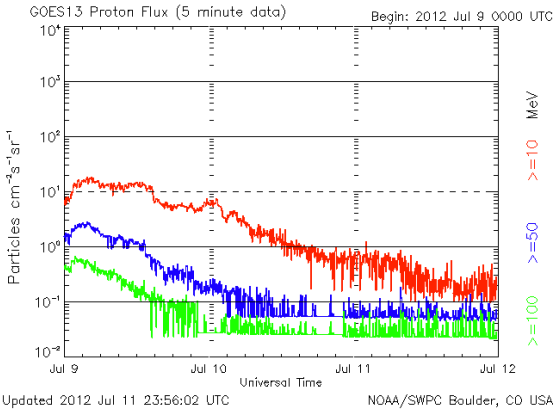

Figure 3. Proton flux measured by the GOES 13 satellite showing quiet geomagnetic condition during the experiments on July 10 and 11, 2012.

3. Numerical Model

The first 1-D unmagnetized model that employs a hybrid approach with fluid electrons and ions and particle-in-cell Monte Carlo Collision (PIC-MCC) dust particles and allows for flexibility in incorporating dynamical charging models for the dust as well as dust mass distributions, is used in this study (Scales, 2004; Chen and Scales, 2005; Mahmoudian and Scales, 2011; Senior et al., 2014). This model is capable of simulating the time evolution of the electron density

irregularities, which corresponds to the radar echoes in all frequency bands associated with polar mesospheric clouds (PMSE) and for all background dusty-plasma parameters. The simulations are corresponding to the coherent radar scattering and fluctuations in dust-plasma are assumed to be at half the radar wavelength. The electron density fluctuations ultimately result in the observed backscattered radar signals. The initial uncharged dust is taken to have an irregular density of the form

$$n_d(x) = n_{d0}\left(1 + \frac{\delta n_d}{n_{d0}} \sin\left(2\pi m x/l\right)\right) \quad (1)$$

where n_{d0} is the undisturbed dust density, δn_d is the dust density irregularity amplitude which is set to 0.2 in the simulation, m is the irregularities mode number and l is the system length in this model. The radar reflectivity is proportional to the electron density fluctuations amplitude in the wavenumber domain ($\delta n_e(k)$) (Royrvik and Smith, 1984). Scales (2004) has shown that for the sinusoidal perturbations used in this model, the radar reflectivity $\eta(k) \propto \delta n_e^2$, where δn_e is the electron density irregularity amplitude.

The one-dimensional mesospheric irregularity model is used in this study for the formation and the time evolution of associated PMSE irregularities in the altitude range around 85 km. At this altitude region the plasma density $n_{e0} = n_{i0} = 2\times10^9$ m^{-3}. The plasma temperature is typically $T_e = T_i = 150^\circ$ K; therefore the electron thermal velocity is $v_{the} \sim 10^5$ m/s. The ion mass is $m_i = 50$ m_p (O_2^+), where m_p is the proton mass. The ions are highly collisional with $\nu_{in} \approx 10^5$ Hz (Mahmoudian et al., 2011). The density irregularities are assumed to have a wavelength of ~ 64 cm, which corresponds to the radar frequency ~ 230 MHz. The photoionization/recombination rates in the equilibrium is $P_i = L_i = \alpha n_{e0} n_{i0}$, $\alpha \sim 10^{-12}$ m^{3}s^{-1} and for typical mesospheric parameters. The production/recombination timescale is of the order of 100 s which is comparable to the ion charging time. Several parameters in the simulations including dust charge density to the background electron density $z_d n_d/n_e$, δn_e^2 (corresponding to radar echoes), and n_e are used in this study. The photo-detachment current included in the charging model is described here (Mahmoudian et al., 2017). The time variation of charge on dust particles based on continuous Orbital-Motion Limited OML approach (Bernstein and Rabinowitz, 1959) can be written as follows:

$$\frac{d_Q}{dt} = I_e + I_i + I_P \quad (2)$$

where I_e, I_i, and I_P are the electron and ion current on each dust particle, and photodetachment current, respectively. Assuming negatively charged dust, photo-detachment current can be approximated by (Rosenberg, 1996)

$$I_{\mathrm{P,Z_d<0}} = -\pi r_d^2 \alpha, \quad (3)$$

For positive grains, photo-detachment current can be approximated by

$$I_{\mathrm{P,Z_d>0}} = -\pi r_d^2 \alpha \exp(\mathrm{q_e}\phi_\mathrm{d}/\mathrm{KT_p}), \quad (4)$$

where r_d is the dust radius, K is the Boltzmann constant, and ϕ_d is dust floating potential. In Eq. (3) and (4), the parameter α is $\alpha = q_e J_p Q_{ab} Y_p$ where q_e, J_p, Q_{ab}, Y_p, and T_p are the electron charge, photon flux, photon absorption efficiency, photoelectron yield, and average photoelectron temperature. Previous studies have estimated solar photon flux J_p to be of the order of $\sim 1.5\times10^5$ photon cm^{-2} s^{-1} for $h\nu \sim$4-5 eV and the absorption efficiency $Q_{ab} \approx 1$ (e.g. Brasseur and Simon, 1981). Photoelectron yield Y_p can also be estimated using $Y_p = C(h\nu - W)^2$, with $C = 0.01/(eV)^2$ (Rapp and Lubken, 1999). Q_{ab} is assumed to be $\sim$1 for $2\pi r_d/\lambda > 1$, where λ is the wavelength of the incident photons (Shukla and Mamun, 2002). Calculations by Rapp (2009) indicate that photo-detachment current is important for sufficiently small radii (1 nm) and metallic compounds (e.g. Fe_2O_3 , SiO). The average photoelectron temperature T_p is assumed to be $\sim 400T_e$ (Mahmoudian et al., 2017). The previous studies have shown that MSP present in the mesosphere may be positively charged due to photoemission by solar UV radiation (Rosenberg and Shukla, 2002). Rosenberg et al., (1996) provided an estimation of photo-emission current for UV intensity of 8-9 eV photon.

The ratio of dust charge density $z_d n_d$ to the background electron density n_e determines the amplitude of the electron density fluctuations. This parameter will be critical for backscattered radar signal to be above the threshold and PMSE to be observable using radars. Therefore, the elevated n_e during EPE, dust density, and dust radius will determine the strength of the backscattered radar signal. The simultaneous increase in electron attachment onto dust particles (n_e decrease) and enhancement of $z_d n_d$ will cause stronger radar echoes. The charging of electrons onto the dust particles will reduce the ambipolar diffusion of electron density fluctuations which results in long-lasting PMSE. Unlike the previous study by Cho and Kelley (1992) that suggests 50% of electrons need to be bound to dust particles in order to observe PMSE, our study shows that with much lower dust density and radius the PMSE should be observed. Previous in-situ rocket measurements and simultaneous PMSE observations have shown PMSE presence for $z_d n_d/n_e > 0.05$ (Rapp et al., 2002 and references therein).

The computational results for the background mesospheric parameters in the quiet mesospheric condition are presented in Figure 4. It should be noted that the irregularities reach the steady state after 200 sec. The dust radius r_d is varied from 2 nm to 20 nm, and dust densities n_d/n_{e0} = 200%, 100%, 50%, 20% are considered. According to the charging model, 20 nm dust particles can collect two electrons on average. As can be seen in Figure 4a, the electron density reduces about 90% for dust particles larger than 10 nm and n_d/n_{e0} = 100%. For smaller dust particles ($r_d \sim$ 2 nm), the reduction in electron density is about the same ($<$ 20%) for n_d/n_{e0} = 100%, 50%, and 20%. The critical parameter of $z_d n_d/n_{e0}$ in mesospheric dusty plasma that determines the strength of VHF PMSE (224 MHz) is shown in Figure 4b. According to this figure, the dust charge density to background plasma density is below the threshold level (0.05) for n_d/n_{e0} = 20% and r_d =2 nm. As the dust radius increases to 20 nm, $z_d n_d/n_{e0}$ increases to 1.4. Another critical aspect of the dusty plasma within PMSE, that has been overlooked in previous studies, is the variation of the amplitude of the electron density fluctuations δn_e as the dusty plasma parameters vary. A comparison of δn_e^2 shown in Figure 4c, which corresponds to the backscatter radar signal amplitude. This figure indicates that measuring the dust charge density $z_d n_d$ normalized to n_e is not sufficient to assess the background mesospheric parameters. Although $z_d n_d/n_{e0}$ increases to 100 and for n_d/n_{e0} = 100% and 50% (Figure 4b), the corresponding radar echoes ($\propto \delta n_e^2$) approach zero (Figure 4c). The maximum amplitude of δn_e^2 for n_d/n_{e0} = 200%, 100%, 50%, and 20% occurs at r_d = 4 nm, 6 nm, 9.5 nm, and 15 nm, and for both $\delta n_d/n_{d0}$ = 0.2. The maximum amplitude of fluctuations (radar echoes) reach 9.61, 9.57, 9.5, and 9.35 log10 m^{-3}, for $n_d = 4\times10^9$, 2×10^9, 10^9, and 4×10^8 m^{-3}, respectively. Therefore, while the required condition $z_d n_d/n_e > 0.05$ for dust densities 100%, 50%, and 20% is satisfied, the radar echoes ($\propto \delta n_e^2$)

are very weak and may be below the threshold level of VHF radar detection. These values for $\delta n_d/n_{d0} = 0.5$ are 10.9, 10.82, 10.82, and 10.6 log10 m^{-3}, for $n_d = 4\times10^9$, 2×10^9, 10^9, and 4×10^8 m^{-3}, respectively. According to observations presented in Figures 1b and 2b, no PMSE is observed near 10.5 log10 N_e m^{-3} which is in agreement with the numerical results presented in Figure 4.

Figures 5 and 6 represent similar parameters including the electron density variation due to charging onto dust particles (n_e/n_{e0} %), $z_d n_d/n_e$, and δn_e^2 for the elevated background electron density by a factor of 10 and 20 ($n_e = 2\times10^{10}$ m^{-3} and 4×10^{10} m^{-3}, respectively). Two values of dust density fluctuation amplitude $\delta n_d/n_{d0}$ of 0.2 and 0.5, and dust density $n_d = 4\times10^9$ m^{-3}, 2×10^9 m^{-3}, and 10^9 m^{-3} are considered in these two figures. Figures 5 shows that the threshold level of $z_d n_d/n_e = 0.05$ for PMSE to be observed by VHF radar is satisfied for $r_d > 4$ nm ($n_d = 4\times10^9$ m^{-3}), $r_d > 8$ nm ($n_d = 2\times10^9$ m^{-3}) and $r_d > 15$ nm (for $n_d = 10^9$ m^{-3}) in the case of $n_e = 4\times10^{10}$ m^{-3}. According to Figure 6, this condition for increased n_e by a factor 20 is $r_d \sim 5$ nm ($n_d = 4\times10^9$ m^{-3}), $r_d > 10$ nm ($n_d = 2\times10^9$ m^{-3}), and $r_d > 17$ nm ($n_d = 10^9$ m^{-3}).

The variation of recombination/photoionization rates is considered in order to study the long-lasting electron precipitation events (case 3 in Figure 2b) as well as short period EPE (Cases 1, 2, 4, and 5 in Figure 2b). As can be seen in Figure 7, the electron density reduces to the value near the natural condition in short period events ($\alpha = 10^{-12}$ m^3 s^{-1}). The difference between the long and short EPE events is mainly prominent for larger dust radius and higher dust densities.

A complete assessment of the required conditions for PMSE observations includes the exact measurements of n_d, r_d, n_e, as well as photoionization/recombination rates, and charging characteristics of dust/ice particles. Therefore, the PMSE existence, time evolution, and strength can be employed to provide an estimation for n_d, r_d, and dust charging characteristics.

4. Discussion

The behavior of PMSE during background electron density enhancement and active geomagnetic condition may have a great potential as a diagnostic for dusty plasma parameters within PMC as well as the formation of ice particles in the polar mesosphere. The main focus of this section is to compare the computational results with the experimental observations in order to develop a remote sensing technique to characterize and measure natural dust layers in the near-Earth space environment. The following sections will investigate the time evolution of PMSE layers observed on July 10 and 11, 2012 and presented in Figures 1 and 2.

4.1. Event 1: July 11, 2012

Case 1 *&* ***2:*** T These two events show the formation of a weak PMSE layer 83–84 km associated with electron density enhancement by a factor of 10 ($n_e \sim 2\times10^{10}$ m^{-3}). As shown in Figure 4, δn_e^2 (backscattered VHF radar signal) in the natural mesospheric conditions is small and decreases significantly as the background dust density n_d reduces. The expected radar echoes are 10.87 and 10.7 $\log_{10}$ N_e m^{-3}. Therefore, non-existence PMSE during natural mesospheric condition is mainly due to the high n_d present in this region. A close comparison with Figure 5b shows that there are three parameter regimes for which the required condition of $z_d n_d/n_e > 0.05$ for the PMSE observation will be satisfied in the enhanced n_e condition by a factor of 10. These parameters for $\delta n_d/n_{d0} = 0.5$ are ($n_d = 4\times10^9$ m^{-3} and $r_d > 4$ nm), ($n_d = 2\times10^9$ m^{-3} and $r_d > 8$ nm), or ($n_d = 10^9$ m^{-3} and $r_d > 15$ nm). The small values of δn_e^2 shown in Figure 5c, validates the weak PMSE observed in cases 1 and 2. According to Figure 5c, these values correspond to the radar echoes ~ 11.3 $\log_{10}$ N_e m^{-3}, which is comparable to the observed radar echoes (Figure 2b). It should be noted that the values of radar echoes associated with $\delta n_d/n_{d0} = 0.2$ are of the order of 10 $\log_{10}$ N_e m^{-3}, which is much weaker than the observed radar echoes. Appearance of PMSE in the course of a very short EPE in cases 1 and 2, and comparison between the value of the estimated radar echoes in the natural mesospheric condition and enhanced electron density by a factor of 10 (10.7–10.87 and ~ 11.3 $\log_{10}$ N_e m^{-3}, respectively), validate the computational results and that the threshold level of VHF PMSE is reached.

Case 3: The time period 3 from 08:50 to 11:00 UT shows the strongest PMSE layer with persistent intensity during EPE, which correlates well with the electron precipitation altitude. The lower layer formed in the altitude range 83–86 km consists of larger particles. The electron density increases by a factor of 15 to 20 throughout this cycle ($n_e = 4\times10^{10}$).

The layer at altitudes closer to mesopause with lower temperature may compose of smaller ice particles and higher densities. The formation of ice particles starts at mesopause altitude where the temperature reaches its minimum. As the ice particles grow through water ligand accumulation, they will settle at lower altitudes due to the action of gravity. The descending in the altitude of this layer between 9:50-10:00 UT and 10:30-10:50 UT may also confirm this hypothesis. The delay in the appearance of this layer could be due to a high ratio of n_d/n_e. This figure shows that the VHF radar echoes reach a maximum amplitude of 12 $\log_{10}$ N_e m^{-3}. A close comparison with the results presented in Figure 6c and for electron density enhancement by a factor of 20, shows that the condition of radar echoes in the order of 12 $\log_{10}$ N_e m^{-3} can be satisfied for one parameter regimes. According to the computational results shown in Figure 6, the expected radar echoes of the amplitude of 12 $\log_{10}$ N_e m^{-3} occurs at $r_d = 10$ nm ($n_d = 4\times10^9$ m^{-3}), and for $\delta n_d/n_{d0} = 0.5$. The computational results also show that this condition is satisfied for $r_d > 20$ nm (for $n_d = 2\times10^9$ m^{-3}), and for $\delta n_d/n_{d0} = 0.5$. Therefore, by taking into account the typical mesospheric conditions, the two parameter sets of ($r_d \sim 10$ nm, $n_d = 4\times10^9$ m^{-3}, $\delta n_d/n_{d0} = 0.5$) is more probable parameters to reproduce the experimental observations shown in Figure 2b and case 3. Another important feature of the computational results presented in Figure 6 is that the radar echoes of 12 $\log_{10}$ N_e m^{-3} satisfied very close to the other requirement of $z_d n_d/n_e$ of 0.05 occurs (Figure 6b), which is estimated based on in-situ rocket measurements and simultaneous VHF PMSE observations on the ground.

According to Figure 2b, a secondary PMSE layer starts to develop at a higher altitude range around 87 km at 09:50 UT and extends to lower altitudes around 86.5 km. This layer is composed of smaller ice particles and larger densities. The delay in appereance also justifies the slow charging process due to smaller charging timescale (Mahmoudian et al., 2011). Based on the simulation results presented in Figure 6, the existence of this layer will require $n_d >\sim 6$–8×10^9 m^{-3} for smaller dust particles ($r_d \sim 2$ nm). The formation of PMSE in higher altitude range 87-88.5 km which corresponds to the smaller dust particles may show a clear signature of newly formed ice cloud with a smaller size (< 3 nm) that are exposed to enhanced electron density and get charged. Another feature to point out is the variation of PMSE strength between 9:30-9:50 UT is due to the saturation of dust particles and enhancement of n_e which results in lower radar reflectivity. The disappearance of PMSE after EPE could be due to the photo-detachment process of electrons from dust particles and recombination with the

background ions. This effect could also be as a result of ice particles destroyed by collision with MSP (< 0.2 nm). As proposed by Rapp et al. (2002), the decay of PMSE can also be explained in terms of the evaporation of ice particles as a result of Joule heating.

Figure 7 shows the variation of $z_d n_d/n_e$ and radar echoes with and without photo-detachment current as well as the variation of recombination rate by a factor of 20. As can be seen, the effect of photo-detachment current and presence of positive dust particles on the required threshold of $z_d n_d/n_e = 0.05$ for VHF PMSE observations and the associated radar echoes is significant. According to the computational results, the minimum dust radius for satisfying $z_d n_d/n_e = 0.05$ condition increases between 4–6 nm, which is much larger than the typical dust particles present in the PMSE region. The effect of photo-detachement current on the associated radar echoes shown in Figure 7b is substantial. This effect is more prominent for larger dust particles. Another parameter that is investigated in Figure 7, is the effect of recombination/photoionization rates enhancement by a factor of 20. This is applicable for long-lasting precipitation event. The changes produced on the minimum dust radius requirement for PMSE observation is ~ 0.5 nm. The estimated backscattered signal amplitude remain unchanged. Therefore, the effect of recombination/photoionization rated on the expected VHF PMSE is very small.

Rapp et al. (2002) argued that the positive correlation of PMSE and electron density enhancement implies a lower limit in electron density. They have also postulated that long-lasting geomagnetic disturbances may increase absolute n_e such that leads to irregularities decrease below the threshold and cause decay of PMSE. This is considered as the upper electron density limit. This paper shows that the correlation of the VHF PMSE presented in Figure 2b and the elevated n_e during long EPE from 8:50-9:30 UT and 10:10-11:10 UT could be due to a wide range of parameters associated with a mesospheric dusty plasma such as n_e, n_d, and r_d.

Case 4 & ***5:*** The cases 4 and 5 show a similar trend to the cases 1 and 2, with the electron density enhancement of the order of $\sim 5 \times n_{e0}$. A close comparison between Figures 5 and 2 indicates that in the case of lower n_e enhancement, the required conditions for the PMSE existence should be satisfied with lower dust densities and smaller dust particles. Therefore, as the electron density increases above the saturation level of dust particles, the electron density fluctuation amplitude increases correspondingly. As discussed, this is mainly due to the dust particles charged up by free electrons, which produce a footprint in the background electron density. The appearance of PMSE layer in such a short EPE confirms that δn_e^2 were very close to the required threshold of VHF PMSE observation (~ 11.3 $\log_{10}$ N$_e$ m^{-3}). This is in agreement with the numerical simulations presented in Figure 4c and 5c, corresponding to the natural and enhances n_e by a factor of 10, respectively.

4.2. Event 2: July 10, 2012

Figure 1b shows the VHF PMSE during several EPE present on July 10, 2012 from 08:00 to 12:00 UT. The two distinct PMSE events are depicted by case 1 and 2. The anti-correlation of the observed VHF PMSE and the enhanced electron density could be attributed to the very low dust density in the region. The observed echoes are very close to mesopause altitude where the condition favor the formation of ice particles as the temperatures reaches its minimum. As can be seen both VHF PMSE occur after the electron precipitation event is ended. The scattered and weak echoes between 09:30 to 10:30 UT could be due to enhanced random fluctuations within enhanced plasma region rather than dust charging process.

4.3. Past PMWE observations during SPE:

The previous study by Kirkwood et al. (2002) has shown the enhanced radar echoes between 50-80 km altitude in the winter mesosphere by the 52 MHz ESRAD radar and during electron precipitation events. The PMWEs are seen in a wide range of background electron densities but limited to the ratio of negative ions to free electrons (~ 100). The low numbers of enhanced PMWE in the presence of SPE could be due to the different charging characteristics of dust particles within PMWE region. It should be noted that water-ice dust particles are less likely to be candidates for dust as the temperatures in the winter mesosphere are too high. The computational results presented in this paper can be applied to PMWE observations.

5. Conclusion

Dusty space plasma diagnosis associated with polar mesospheric clouds (PMC) is investigated using the behavior of polar mesospheric summer echoes (PMSE) during electron precipitation event. The two consecutive day observations of PMSE using 224 MHz VHF radar at EISCAT during electron precipitation event (EPE) on July 10 and 11, 2012 have been presented. The Virginia Tech dusty plasma computational model capable of simulating the time evolution electron density fluctuation in the presence of natural mesospheric dust layers and the corresponding radar echoes (PMSE) in different frequency bands is employed in this study. The effect of several parameters including dust radius r_d, dust density n_d, recombination/photoionization rates, on background plasma on the associated radar echoes is investigated. It has been shown for the first time that the dust density and dust radius limit within PMSE region can be understood by studying the evolution of radar echoes including existence of PMSE layer, duration of the echoes, correlation with EPE, as well as the strength of the backscattered signal. While electron density plays an important in $(\delta n_e)^2$ corresponding to the radar echoes, the results presented in this paper show that the PMSE strength is mostly governed by background dusty plasma parameters such as dust radius and dust density.

A comparison of the PMSE observations during short period EPE with elevated electron number densities $\sim 2 \times 10^{10}$ ($10 n_{e0}$ background electron density) reveals the existence of ice particles in the polar summer mesopause region about $n_d > 4 \times 10^9$ m^{-3} and $r_d > 2$ nm. A comparison of the numerical simulations in the natural mesospheric conditions and the enhanced electron density by a factor of 10 shows that the minimum requirement of $\delta n_d/n_{d0} = 0.5$, which is based on the past VHF PMSE observation and simultaneous in-situ rocket measurement, is satisfied for the $n_d = 4 \times 10^9$ m^{-3} and $r_d > 4$ nm. The estimated radar echoes are ~ 10.8 and 11.3 in the natural and enhanced n_e conditions, respectively. This validates the appearance of VHF PMSE during short EPE. The long-lasting PMSE enhancement correlated with EPE on July 11, 2012, imposes a lower limit of $n_d >\sim 8 \times 10^9$ m^{-3} and $r_d >\sim 2$ nm. The computational results associated with radar echoes of 12 $\log_{10}$ N$_e$ m^{-3} revealed the conditions of $n_d = 4 \times 10^9$ m^{-3} and $r_d \sim 10$ nm. Considering that this layer appreas in the lower altitudes (83–85 km) validates the numerical results which impose a minimum dust radius of 10 nm for VHF PMSE observations. The secondary PMSE layer formed at higher altitude range of 86.5–88 km is composed of smaller ice particles. The delay in the formation of this layer is due to the slow charging process of small dust particles. The numerical simulations require a much higher dust densities (6–8$\times 10^9$ m^{-3} and $r_d \sim$ 2 nm) for VHF PMSE observations in this altitude range and with a strength ~ 12 $\log_{10}$ N$_e$ m^{-3}. The weak VHF PMSE

observed on July 10, 2010 show anti-correlation with the elevated electron density due to EPE. This was attributed to the very low dust density present in this region. The negative correlation between electron density enhancement and radar echoes is due to the limited amount of dust particles present in the region. In summary, the dusty plasma simulations will be sufficient to interpret the PMSE behavior during EPE or solar proton event (SPE) and can lead to significant diagnostics of the dust layer.

The model predicts a stronger PMSE $\sim$ 1 $\log_{10}$ N_e m^{-3} for long-lasting EPE in comparision with short period EPE, which is consistent with the experimental observations. This validates the diagnostic information resulted from the comparison of the PMSE variation during EPE with the computational results. The variation of recombination/photoionization rates by a factor of 10 may introduce 0.1–0.5 nm difference in the minimum required condition ($z_d n_d/n_e = 0.05$) to observe VHF PMSE, which is negligible. This effect on the associated radar echoes is negligible. The disappearance of PMSE is explained of three possible processes including photo-detachment of electrons from dust particles and recombination process, collision with small MSP, and ice particle evaporation due to Joule heating.

The condensation of nuclei of the ice particles such as proton hydrate clusters ($H^+(H_2O)_n$) or meteoric smoke particles (MSP) can be determined by employing microphysical simulations. This can resolve the discrepancy in the description of the observed phenomena. The possibilities of combining the Virginia Tech dusty plasma model with NCAR WACCM/CARMA (Whole Atmosphere Community Climate Model/Community Aerosol and Radiation Model) to develop a large aperture radar simulator for dusty space plasma in the near Earth space environment is currently under investigation. In this approach the background mesospheric parameters will be incorporated in the micro-physics simulations in order to derive the ice/dust density profile and dust size distribution, which will be imported to the dusty plasma model for corresponding radar echoes calculations. To provide a better explanation of the PMSE during active geomagnetic event and use this as a naturally modified mesospheric condition, the new EISCAT 3D interferometry capability will be implemented in the future in order to develop a remote sensing technique for the background mesospheric parameters.

Acknowledgments. This work was partially supported by National Science Foundation (NSF). The EISCAT is an international association supported by research organizations in China (CRIRP), Finland (SA), Japan (NIPR and STEL), Norway (NFR), Sweden (VR), and the United Kingdom (NERC). The data presented in this paper can be downloaded from the EISCAT online database at https://www.eiscat.se/scientist/data/

References

Balsley, B. B., Ecklund, W. L., and Fritts, D. C.: VHF echoes form the high-latitude mesosphere and lower thermosphere: observations and interpretations, J. Atmos. Sci., 40, 24512466, 1983.

Brasseur, G., and P. C. Simon, Stratospheric chemical and thermal response to long-term variability in solar irradiance, J. Geophys. Res., 86, 7343-7362, 1981.

Bernstein, I.B., and Rabinowitz I.N. (1959), Theory of electrostatic probes in a low density plasma Phys. Fluids 2 11221

Chen, C., and W. A. Scales (2005), Electron temperature enhancement effects on plasma irregularities associated withcharged dust in the Earths mesosphere, J. Geophys. Res., 110, A12313, doi:10.1029/2005JA011341.

Cho, J. Y. N. and Kelley, M. C.: Enhancement of Thomson scatter by charged aerosols in the polar mesosphere: measurements with a 1.29-GHz radar, Geophys. Res. Lett., 19, 10971100, 1992.

Christon, S. P., Hamilton, D. C., Plane, J. M. C., Mitchell, D. G., Grebowsky, J. M., Spjeldvik, W. N., Nylund, S. R. (2017). Discovery of suprathermal ionospheric origin Fe+ in and near Earth's magnetosphere. Journal of Geophysical Research: Space Physics, 122, 11,17511,200. https://doi.org/10.1002/2017JA024414

Ecklund, W. L. and Balsley, B. B.: Long-term observations of the arctic mesosphere with the MST radar at Poker Flat, Alaska, J. Geophys. Res., 86, 77757780, 1981.

Eremenko, M. N., S. V. Petelina, A. Y. Zasetsky, B. Karlsson, C. P. Rinsland, E. J. Llewellyn, and J. J. Sloan (2005), Shape and composition of PMC particles derived from satellite remote sensing measurements, Geophys. Res. Lett., 32, L16S06, doi:10.1029/2005GL023013.

Gelinas, L. J., K. A. Lynch, M. C. Kelley, R. L. Collins, M. Widholm, E. MacDonald, J. Ulwick, and P. Mace (2005), Mesospheric charged dust layer: Implications for neutral chemistry, J. Geophys. Res., 110, A01310, doi:10.1029/2004JA010503.

Havnes, O., de Angelis, U., Bingham, R., Goertz, C. K., Morfill, G. E., and Tsytovich, V.: On the role of dust in the summer mesopause, J. Atmos. Terr. Phys., 52, 637643, 1990

Havnes O. and Brattli A. and Aslaksen T. and Singer W. and Latteck R. and Blix T. and Thrane E. and Trim J. (2001), First common volume observations of layered plasma structures and polar mesospheric summer echoes by rocket and radar, Geophys. Res. Lett., 28, 1419–1422

Hervig, M. E., R. E. Thompson, M. McHugh, L. L. Gordley, J. M. Russell III, and M. E. Summers (2001), First confirmation that water ice is the primary component of mesospheric clouds, Geophys. Res. Lett., 28, 971–974.

Hervig, M. E., Gordley, L. L., Stevens, M. H., Russell, J. M., Bailey, S. M., and Baumgarten, G.: Interpretation of SOFIE PMC measurements: Cloud identification and derivation of mass density, particle shape, and particle size, J. Atmos. Solar. Terr. Phys., 71, 316330, doi:10.1016/j.jastp.2008.07.009, 2009.

Hunten, D. M., R. P. Turco, and O. B. Toon (1980), Smoke and dust particles of meteoric origin in the mesosphere and stratosphere, J. Atmos. Sci., 37, 1342 1357.

Jarvis, M. J., M. A. Clilverd, M. C. Rose, and S. Rodwell (2005), Polar mesosphere summer echoes (PMSE) at Halley (76 S, 27 W), Antarctica, Geophys. Res. Lett., 32, L06816, doi:10.1029/2004GL021804.

Kirkwood, S., Barabash, V., Belova, E., Nilsson, H., Rao, N., Stebel, K., Osepian, A., and Chilson (2002), P. B.: Polar mesosphere winter echoes during solar proton events, Adv. Pol. Up. Atmos. Res., 16, 111125.

Mahmoudian, A., W. A. Scales, M. J. Kosch, A. Senior, and M. Rietveld (2011), Dusty space plasma diagnosis using temporal behavior of polar mesospheric summer echoes during active modification, Ann. Geophys., 29, 21692174, doi:10.5194/angeo-29-2169-2011.

Mahmoudian, A., A. R. Mohebalhojeh, M. M. Farahani, W. A. Scales, and M. Kosch (2017), Remote sensing of mesospheric dust layers using active modulation of PMWE by highpower radio waves, J. Geophys. Res. Space Physics, 122, 843856, doi: 10.1002/2016JA023388.

Rapp, M., and F. J. Lubken, Modeling of positively charged aerosols in the polar summer mesopause region, Earth Planets Space, 51, 799 807, 1999.

Rapp, M., Gumbel, J., Lubken, F.-J., and Latteck, R. (2002): D-region electron number density limits for the existence of polar mesosphere summer echoes, J. Geophys. Res., 107 (D14), doi:10.1029/2001JD001323, 2002.

Rapp, M. and F.J. Lubken (2004), Polar mesosphere summer echoes (PMSE): Review of observations and current understanding, Atmos. Chem. Phys., 4, 26012633.

Rapp, M., Charging of mesospheric aerosol particles: the role of photodetachment and photoionization from meteoric smoke and ice particles, Annales Geophys. 27, 24172422, 2009.

Rapp M, Strelnikova I, Li Q, Engler N, and Teiser G., (2013), Charged Aerosol Effects on the Scattering of Radar Waves from the D-Region, Climate and Weather of the Sun-Earth System (CAWSES), Chapter 19 (doi:10.1007/978-94-007-4348-919)

Reid, G. C. (1997), On the influence of electrostatic charging on coagulation of dust and ice particles in the upper mesosphere, Geophys. Res. Lett., 24(9), 1095 1098.

Robertson, S., et al. (2009), Mass analysis of charged aerosol particles in NLC and PMSE during the ECOMA/MASS campaign, Ann. Geophys., 27, 12131232.

Rosenberg, M., J. Vac. Sci. Technol., Ion-dust streaming stabilities in processing plasmas, 14, 631, 1996

Rosenberg, M., and P. K. Shukla, Dust-acoustic-drift wave instability in a space dusty plasma, J. Geophys. Res., 107(A12), 1492, doi:10.1029/2002JA009539, 2002.

Royrvik, O., and L. G. Smith (1984), Comparison of mesospheric VHFradar echoes and rocket probe electron concentration measurements,J. Geophys. Res., 89, 9014.

Scales, W. (2004), Electron temperature effects on small-scale plasma irre-gularities associated with charged dust in the Earths mesosphere, IEEETrans. Plamsa Sci., 32, 724.

Scales, W.A. and Mahmoudian, A. (2016), Charged dust phenomena in the near Earth space environment, Reports on Progress in Physics, Vol 79, No 10, http://dx.doi.org/10.1088/0034-4885/79/10/106802.

Senior, A., A. Mahmoudian, H. Pinedo, C. La Hoz, M. T. Rietveld, W. A. Scales, and M. J. Kosch (2014), First modulation of high-frequency polar mesospheric summer echoes by radio heating of the ionosphere, Geophys. Res. Lett., 41, 53475353, doi:10.1002/2014GL060703.

Shukla, P. D., and A. A. Mamun (2002), Introduction to Dusty Plasma Physics, Inst. of Phys., Bristol, U. K.

Corresponding author: Alireza Mahmoudian (alirezam@vt.edu)

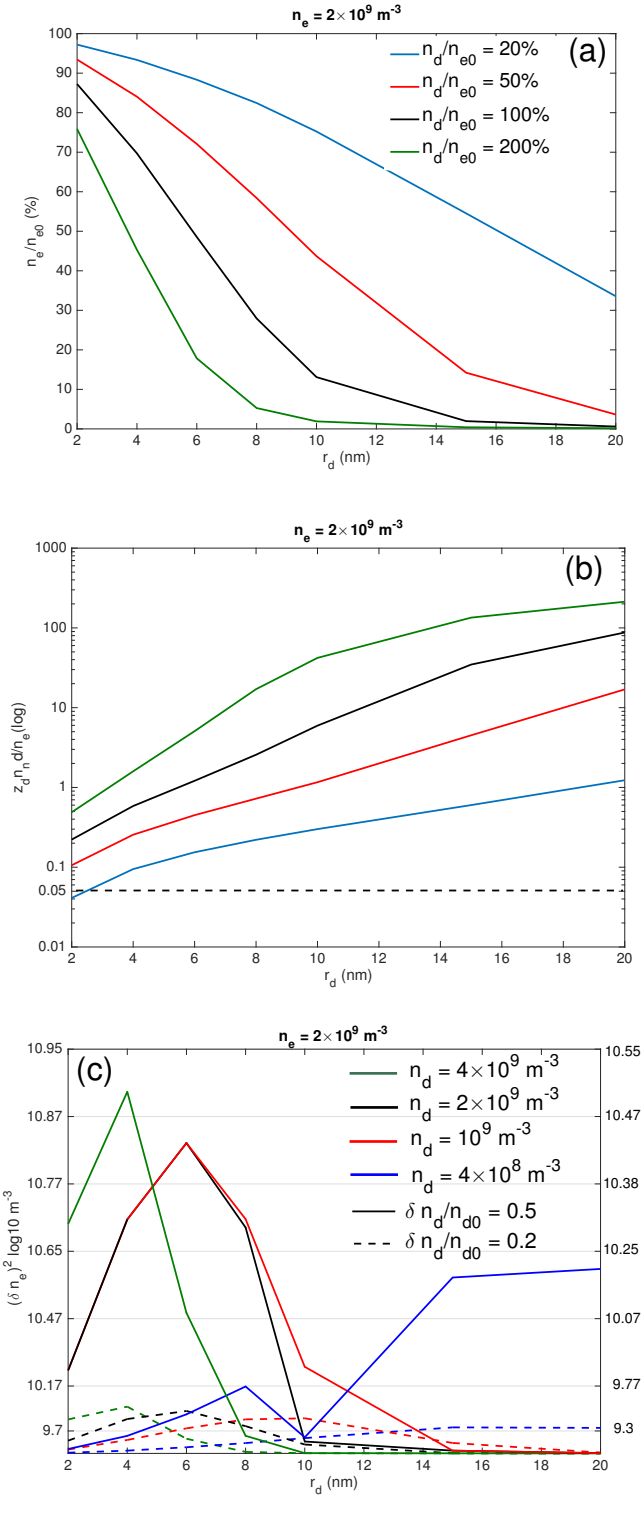

Figure 4. Variation of polar mesospheric summer echoes (PMSE) during quiescent mesospheric conditions with dust radius and dust densities a) steady-state electron density relative to the background electron density b) dust charge density relative to background plasma density c) Steady-state plasma density in the presence of dust particles. The unit is calculated for the dust density of 100%. For dust densities (n_d/n_{e0}) 200%, 50%, and 20%, the values should be adjusted by +0.3, -0.3, and -0.7, respectively.

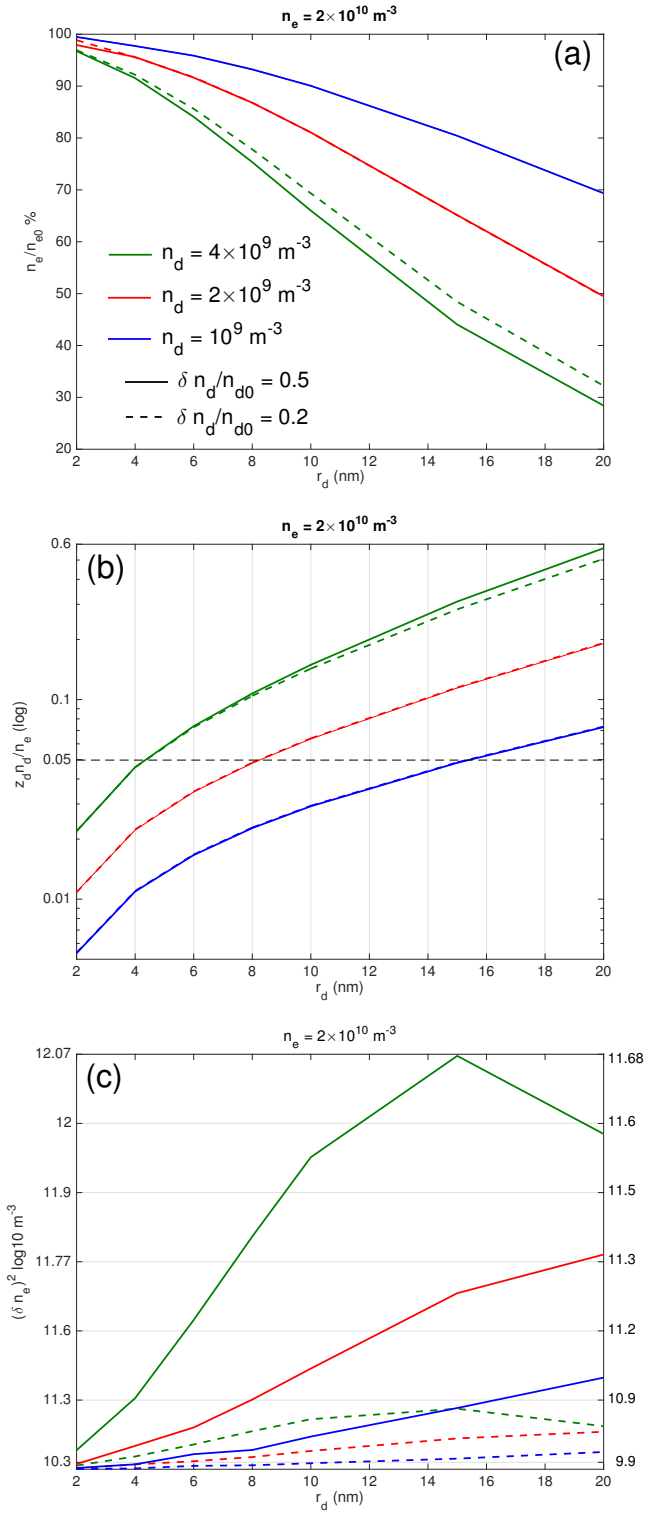

Figure 5. Variation of polar mesospheric summer echoes (PMSE) with dust radius and dust densities during EPE and for enhanced $n_e = 2 \times 10^{10}$ m^{-3} a) steady state electron density relative to the background electron density b) dust charge density relative to background plasma density c) Steady-state plasma density in the presence of dust particles. The units on the left is calculated for the dust density 4×10^9 m^{-3} and $\delta n_d/n_{d0} = 0.5$, and the units on the right corresponds to $\delta n_d/n_{d0} = 0.2$. For dust densities $n_d = 2 \times 10^9$ and 10^9 m^{-3}, the values should be adjusted by -0.3 and -0.6, respectively.

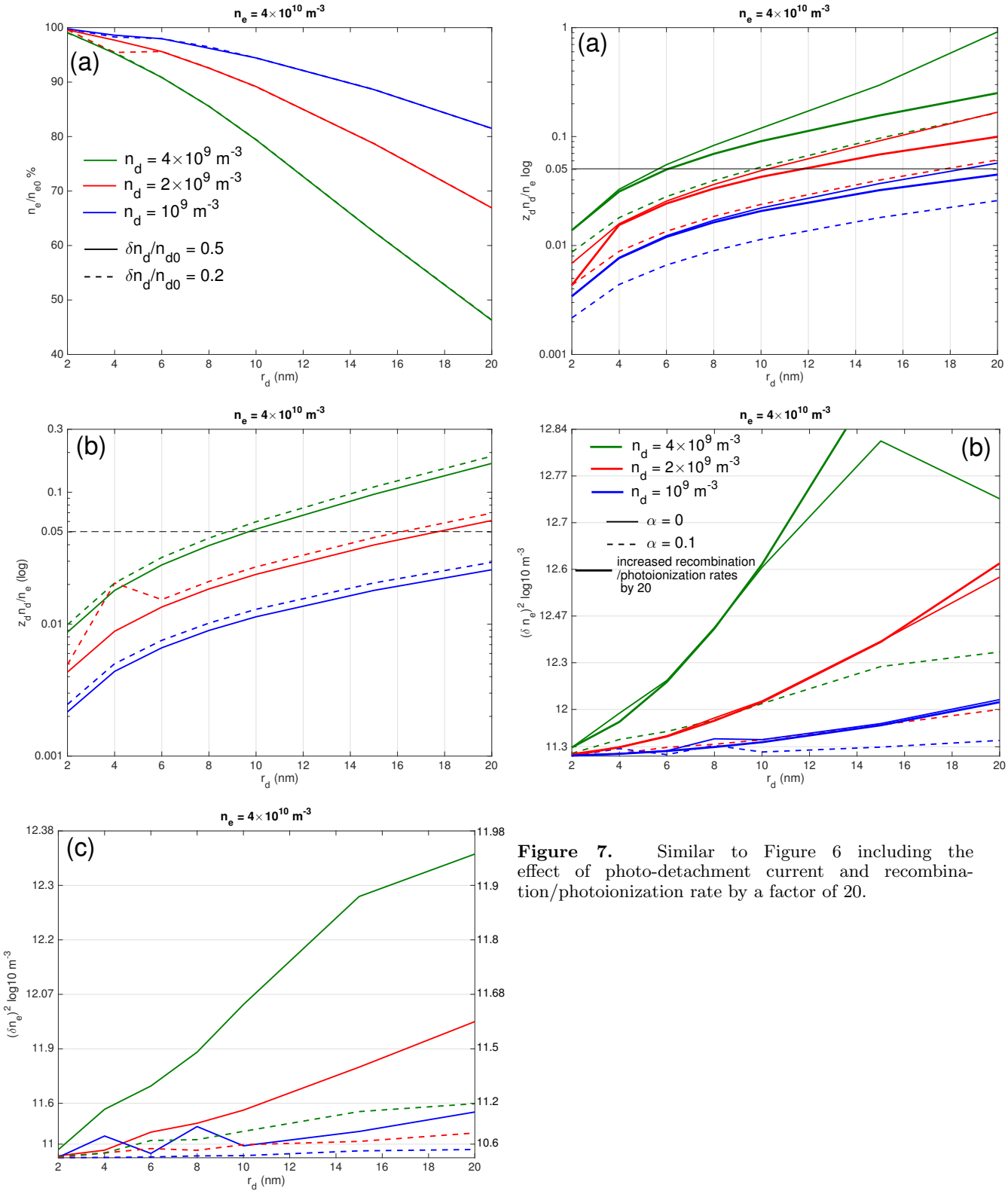

Figure 6. Variation of polar mesospheric summer echoes (PMSE) with dust radius and dust densities during EPE and for enhanced $n_e = 4 \times 10^{10}$ m^{-3} a) steady-state electron density relative to the background electron density b) dust charge density relative to background plasma density c) Steady-state plasma density in the presence of dust particles. The units on the left is calculated for the dust density 4×10^9 m^{-3} and $\delta n_d/n_{d0} = 0.5$, and the units on the right corresponds to $\delta n_d/n_{d0} = 0.2$. For dust densities $n_d = 2 \times 10^9$ and 10^9 m^{-3}, the values should be adjusted by 0.3 and 0.6, respectively.

Figure 7. Similar to Figure 6 including the effect of photo-detachment current and recombination/photoionization rate by a factor of 20.